Supporting Information

Guo *et al.* 10.1073/pnas.0807596106

SI Text

Cutting Procedure for SWNT Electrode Formation. After device fabrication and characterization, a PMMA layer (950, A2) was spincast (4000 PRM, 45 s) on the surface and then baked at 170 °C for 2 min. Using e-beam lithography, we run a DesignCAD file with ≈5-nm-width line at the specific position to obtain the window precursor. Then the mixture of water/isopropanol (1:3) is used for the liftoff at 5 °C for 1 min with the aid of sonication. After liftoff, the devices were washed by DI water and dried with a stream of N_2 gas. After the window was opened, the devices were put into a TECNIQUES Series 800 RIE machine. The nanotubes were then locally cut through the open window by oxygen plasma (50 W RF power, oxygen 250 mTorr, for 10 s). After cutting, the devices were soaked in acetone solution overnight, removed, washed by acetone, isopropanol, and deionized water and dried with a stream of N_2 gas. Under these optimized conditions, ≈20–25% of the tubes were completely cut. Based on the previous results, the statistical variability of the plasma etch process creates ensembles of nanotube devices with gaps in the 1- to 10-nm range. Parts of the devices were used further to fabricate the devices with SWNT-Metal junctions protected by HSQ using e-beam lithography according to our previous report.

Current–Voltage Curves for a Device Made by Drop-Casting. See Fig. S1.

Device Characteristics for a Metallic Device. See Fig. S2.

Power-Dependence Experiment. See Fig. S3.

Wavelength-Dependence Experiment. To further understand the important role of HBCs in device photoconductivity, we intend to display the wavelength dependence measurement of the devices. In the source-drain current (I_{sd}) vs. wavelength experiments, the device was illuminated with visible light (370–700 nm) coming from a xenon lamp (Oriel Instruments). The light was collimated and focused with mirrors and lens from Newport Corporation and diffracted with monochromator of ISA Instruments. The outcoming light was filtered with a long-pass filter (>365 nm) to eliminate double-light phenomena. The light power was measured with 1830C Newport power meter. Source and drain potentials were applied to the transistor with 2 source meters (2400; Keithley), functioning as a semiconductor parameters analyzer. The photocurrent was measured by the Keithley source meters. The various instruments (monochromator, source meters) were controlled by a home-made Labview program (National Instruments) as well as the data collection using a PC.

The current responses as a function of light wavelength of a device made by drop-casting have been shown in Fig. S4 while the device is held at −20-V source-drain bias and 0-V gate bias. The red curve shows the results of the wavelength-dependence experiments. The black curve indicates the UV/vis absorption spectrum of HBC thin films on quartz. The peaks of the photocurrent spectral response of the device at ≈400 nm match those of the UV/vis absorption spectrum of HBC thin films due to the "radialene" π–π^* transitions. Because of the combinations of vibronic excitations, there are several overlapping peaks. The weak peaks at >450 nm in the red curve are most likely due to (radialene π) − (radialene π^*) triplets. These results clearly prove that self-assembled columnar nanostructures of HBC molecules play the key role in device characteristics.

Current–Voltage Curves for a Device Made from 6,13-di(2′-thienyl)pentacene. See Fig. S5.

Current–Voltage Curves for Another Device Made from 6,13-di(2′-thienyl)pentacene. See Fig. S6.

Photoresponsibility for the Same Device as in Fig. S6. See Fig. S7.

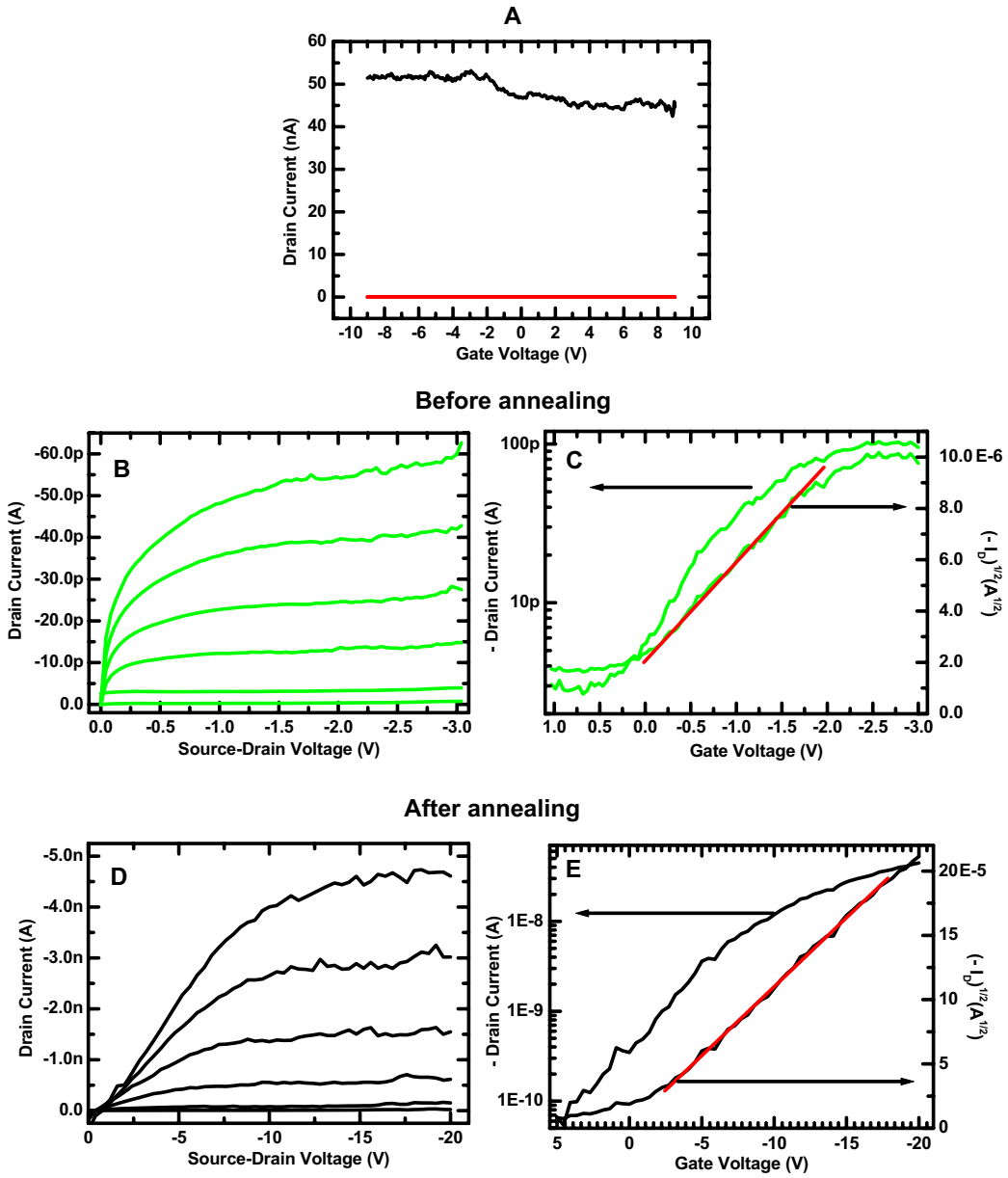

Fig. S1. Device characteristics of a device made by drop-casting before and after annealing. (*A*) Electrical characteristics of a metallic tubes (I_D vs. V_G at V_D = 50 mV) used for testing before (black curve) and after (red curve) oxidative cutting. (*B*) Transistor output, V_G = 0 to −3 V in 0.6-V steps. (*C*) Transfer characteristics for the device, V_D = −3 V. (*D*) Transistor output, V_G = 0 to −20 V in 4-V steps for the same device after heat treatment. (*E*) Transfer characteristics for the device, V_D = −20 V.

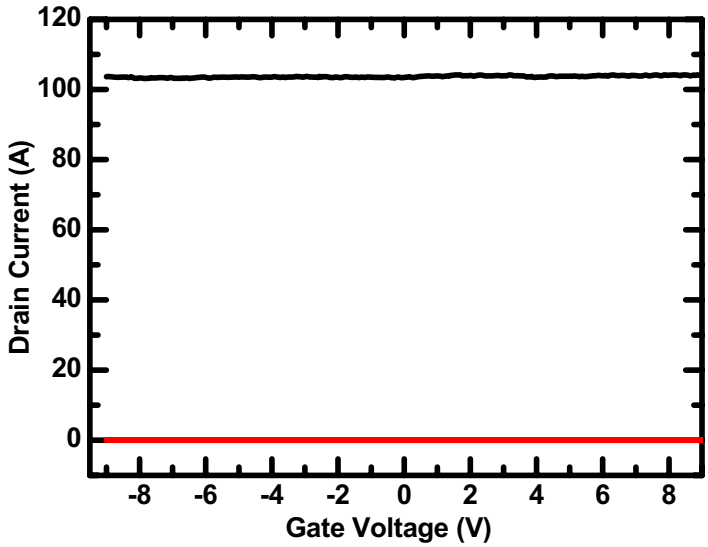

Fig. S2. Electrical characteristics of a metallic tube (I_D vs. V_G at $V_D = 50$ mV) used for testing in Fig. 4 before (black curve) and after (red curve) oxidative cutting.

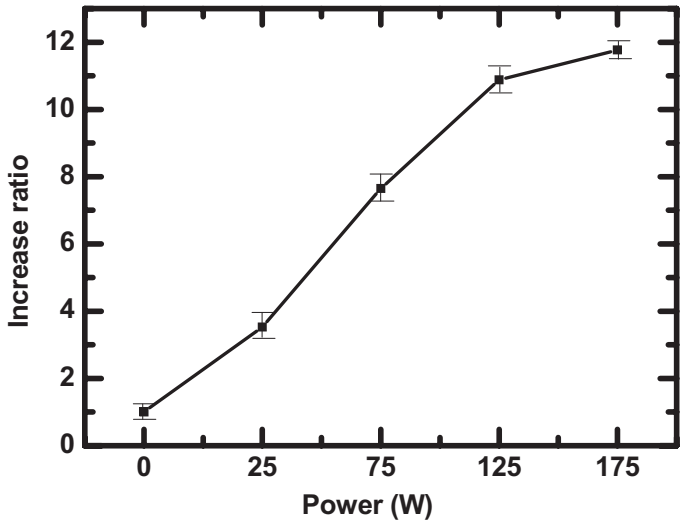

Fig. S3. The power dependence of the photocurrent of a device when the power of the halogen lamb was gradually increased to its maximum while the source-drain and gate voltage bias was fixed at −20 V. With the increase of light power, the drain current of the device gradually saturates, indicating that the photo-induced carrier density reaches its maximum.

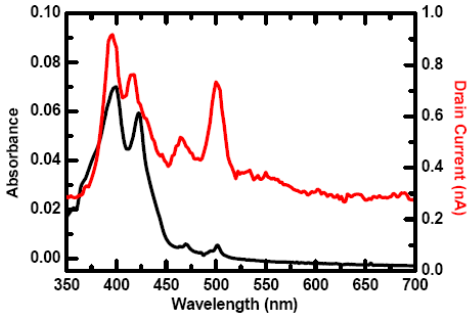

Fig. S4. Demonstration of the wavelength dependence of a device made by drop-casting. The red curve shows the wavelength dependence of the current responses of the device while the device is held at −20-V source-drain bias and 0-V gate bias. The black curve shows the UV/vis absorption spectrum of HBC thin film on quartz.

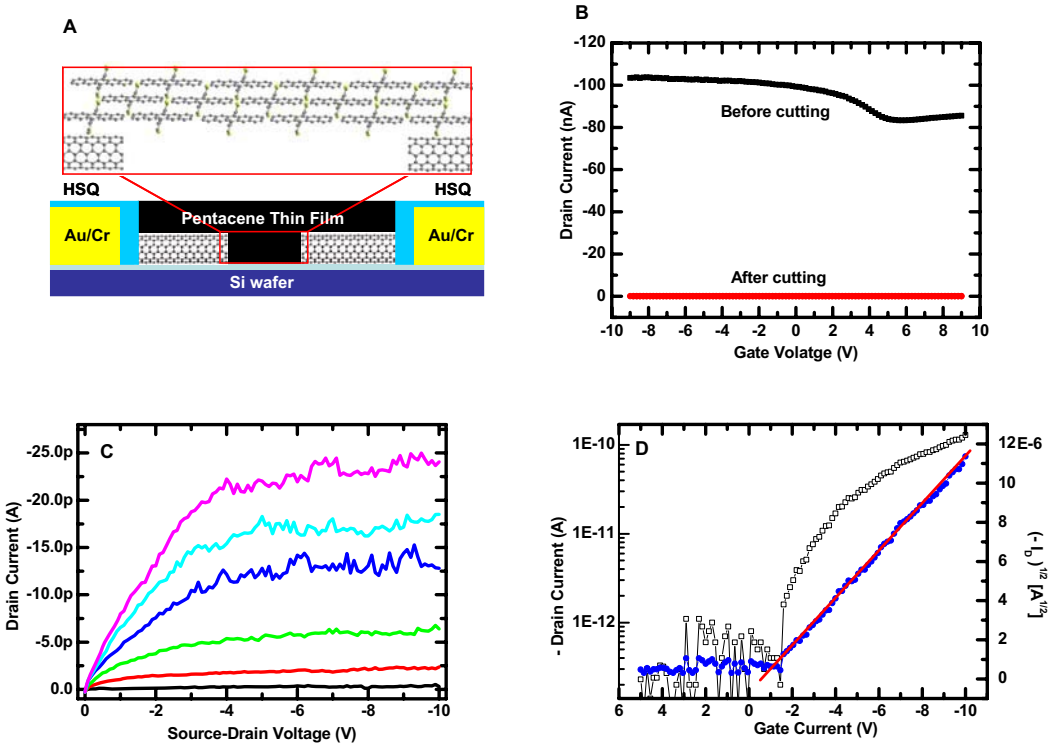

Fig. S5. All of the working devices exhibit the typical *p*-type FET properties. (*A*) The schematic of the device structure used for testing 6,13-di(2′-thienyl)pentacene with SWNT–molecule junctions protected by HSQ. (*B*) Electrical characteristics of a metallic tube (I_D vs. V_G at V_D = 50 mV) used before (black curve) and after (red curve) oxidative cutting. (*C*) Transistor output of the same device, V_G = 0 to −10 V in 2-V steps. (*D*) Transfer characteristics for the device, V_D = −10 V.

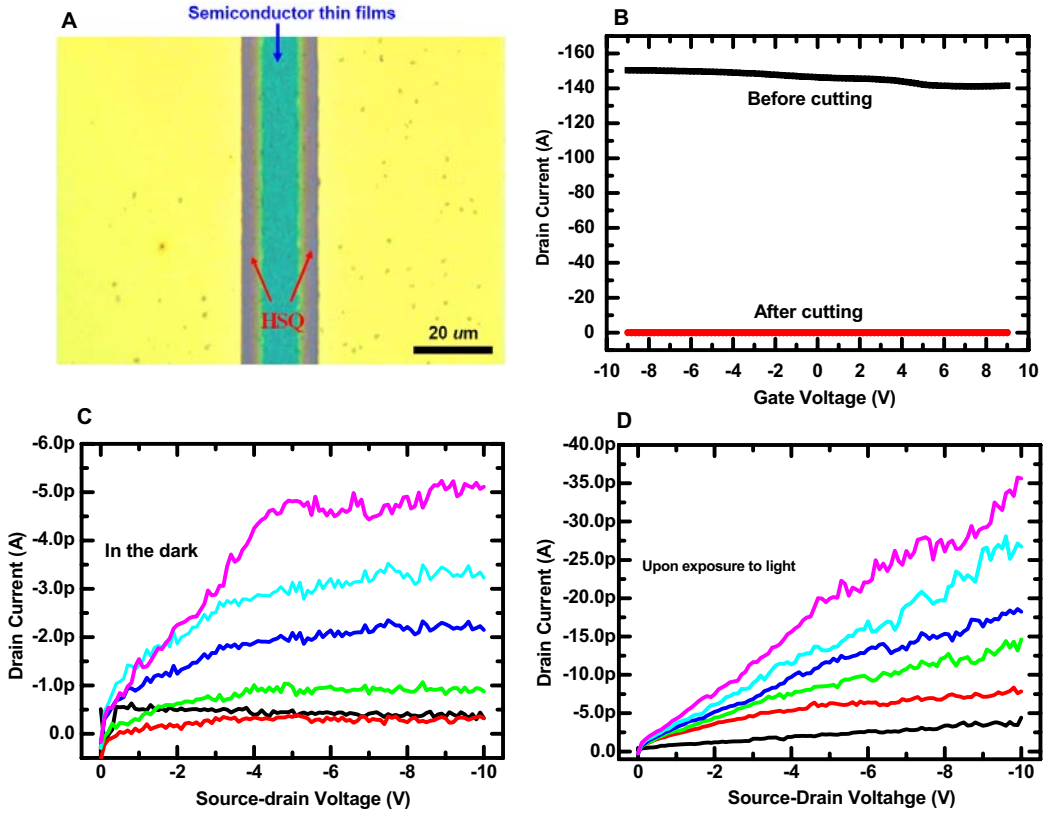

Fig. S6. Device characteristics of another device made from 6,13-di(2′-thienyl)pentacene. (*A*) An optical photograph of a device used for testing 6,13-di(2′-thienyl)pentacene with SWNT–metal junctions protected by HSQ. (*B*) Electrical characteristics of a metallic tube (I_D vs. V_G at $V_D = 50$ mV) used before (black curve) and after (red curve) oxidative cutting. (*C*) Transistor output, $V_G = 0$ to -10 V in 2-V steps in the dark. (*D*) Transistor output, $V_G = 0$ to -10 V in 2-V steps under light irradiation.

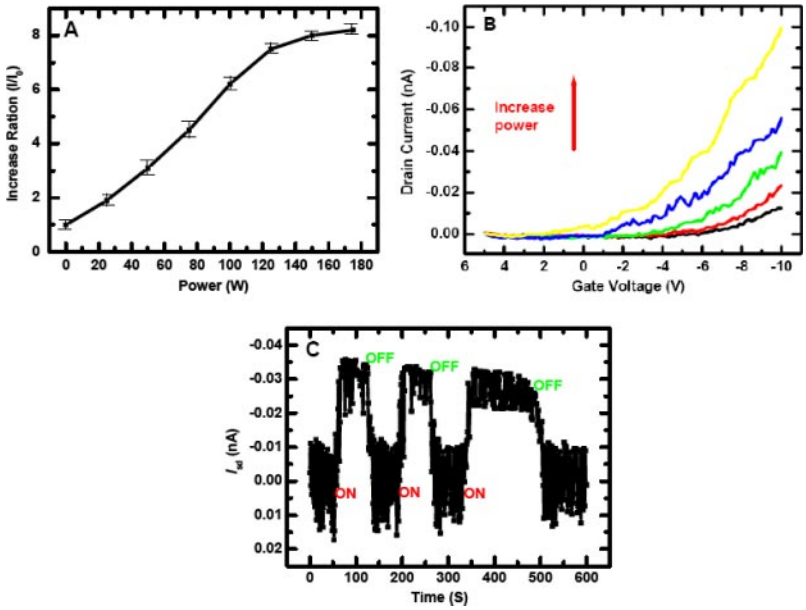

Fig. S7. Photoresponsive behaviors of the same device in Fig. S6. (*A*) The power dependence of the photocurrent of the same device measured in Fig. S6 when the power of the halogen lamb was gradually increased to its maximum while the source-drain and gate voltage bias were fixed at −10 V. (*B*) Transfer characteristics of the same device with the increase of light power. (*C*) The drain current as a function of time while the same device is held at −10-V source-drain bias and −10-V gate bias by switching on/off light.